

Application of Cutting-Edge 3D Seismic Attribute Technology to the Assessment of Geological Reservoirs for CO₂ Sequestration

Type of Report: Progress

Frequency of Report: Quarterly

Reporting Period: July 1, 2009 – September 30, 2009

DOE Award Number: DE-FG26-06NT42734 [University Coal Research] (UH budget G091836)

Submitting Organizations: Department of Earth and Atmospheric Sciences
Reservoir Quantification Lab
University of Houston
Houston, Texas 77204-5505

Preparers: Prof. Christopher Liner - P.I.
Dr. Jianjun (June) Zeng
Dr. Po Geng
Heather King (coordinator for this report)
Jintan Li
Phone: 713-743-919
Fax: 713-748-7906

CONTENTS

Executive Summary	3
Geology	4
Geophysics	10
Reservoir Simulation.....	16
Work Plan for the Next Quarter	18
Cost and Milestone Status.....	20
Summary of Significant Events	21
Technology Transfer Activities.....	22
Contributors.....	22
Tables.....	23
Figures	24

Executive Summary

The Dickman field project has made good progress in geology, geophysics, and flow simulation.

In geology, the structural model has taken final form and this, in turn, has been propagated to the simulation grid. We are still making final investigations of the value and accuracy of various seismic attributes in relation to the structural model. The reservoir property model is near completion, although further work with the large amount of borehole data is possible. The beginnings of a geological history of the area were undertaken in this quarter with an eye toward the final project report.

Geophysical work focused on higher-accuracy synthetic seismograms, structural analysis of the Ft. Scott (as regional seal), seismic inversion, and conversion of flow simulator output to time-lapse (4D) seismic data. The latter effort would allow scenarios to be tested about seismic visibility of CO₂ injection, retention, and leakage at mid-continent US sites like Dickman. This will likely be further developed through future funding opportunities.

Flow simulation has been the major effort in this quarter. We have made good progress on construction of flow grids, history matching to field data, convergence testing using local grid refinement, and assessment of pressure regimes during the simulated injection process. Our simulations have typically run for a 25 year initial injection phase, followed by 225 year simulation period.

We are also pleased to report that a DOE-funded \$300K follow-on project has been awarded to the University of Houston. This is a 2-year training project that will allow us to keep our fledgling CO₂ team together, recruit two additional students, and participate in future funding opportunities.

Activities in Quarter

Geology

Major progress in structural and petrophysical modeling using Petrel include improved understanding of lithological and structural controls on the reservoir conductivity by litho-zone mapping and an improved data-processing work flow for the porosity and permeability computation in the property modeling using all sources of data. This resulted in two structure and property grids serving as input data sets to the CMG simulator: a layer-averaged property model for the history-match simulation and a more complicated 16-layer model for the CO₂ injection simulation. The former focused on the two depleted reservoirs within the seismic survey boundary with good well-control, and the later extrapolated results from the former to the entire stratigraphic section.

We have established a better geological fault/fracture system as a result of interpreting “sub-seismic” structural features using multiple seismic attributes. This framework will provide better control for reservoir conductivity in simulating grids.

Structure modeling

Stratigraphic framework and lithologic zonation

Litho-zone logs for 39 wells were constructed based on geology reports, log interpretation and core descriptions from the nearby Schaben Field, as shown in Figure 1. The base map in Figure 1 is contoured over the major fold structure for the Pennsylvanian to Mississippian strata. Figure 2 is a representative well cross-section showing correlation of litho-zonations. All sections are hung on the Fort Scott formation top. This lithological framework served as a base for the calibration of neutron porosity logs by lithology in the petrophysical modeling (next section). The porosity readings need to be corrected in the following lithologic units: the coal-bearing Pennsylvanian Cherokee Group sandy-shaly interbeds, the Pennsylvanian Cherokee Sandstone sandy beds including the Lower Cherokee cherty conglomerates, and the Mississippian Salem, Warsaw, and Osage cherty dolomite. The last group tends to have higher porosity values than reflected by the neutron porosity logs scaled on limestone matrix. The Fort Scott

Limestone and the Base-Penn Limestone are treated as pure limestone units, due to limited lithologic descriptions. No corrections were made on these two units, regardless of a muddy-shaly interbed existing in the former and the varying lithology for the latter over the entire studied area.

Data QC on input structural model for the CMG flow simulation

Well litho-zone data are used to validate the CMG flow simulation grid over its two center-lines (Figure 3): a) W-E center line along Y=697500, and b) N-S center line along X=1570000. The red dot in Figure 3 indicates the simulated CO₂ injector at the intersection of the two center lines. Figure 4 shows the litho zones along the two center lines of the grid used in CMG flow modeling. The wells on the W-E center line section did not penetrate the deep saline aquifer. The well-control on the center lines shows a good match between litho-zones (labeled in the color bar) created from well tops (in depth domain) and litho-zones derived from combined geology and depth-converted seismic using the latest M3 property model. However, the non-reservoir zone seen in some wells (from 0 to 20 feet) immediately below the Mississippian Unconformity in the M3 model is thicker than seen in zone logs and from well tops, probably due to the resolution of the seismic for a layer with significant lateral variation in thickness. The above zonation framework is used to generate a zone-averaged porosity and permeability models for the history-matching process.

For the CO₂ injection modeling, the above framework is further divided into 16 zones. In Figure 5, each layer in Figure 4 is divided into sub-layers with equal thickness, based on the analysis of property distribution, resulting in a 16-layer input data set. Well litho-zone logs are overlain on the sections and validated section by section and layer by layer, to ensure that the framework used in flow simulation reflects as much as possible the real subsurface geology, before any necessary up-scaling and simplification based on the computing capacity.

Petrophysical Modeling

Work flow for porosity log calibration

Figure 6 shows the work flow and the risk assessment in processing raw data from various sources for porosity and permeability modeling. The words in black squares

indicate the raw data from cores (core permeability and porosity), logs (neutron porosity, density and velocity), as well as core measurements within the same stratigraphic target from other Fields. Green arrows connect steps of data correction and calibration (numbers within circles), before the data can be used as the input for the next step. The blue squares represent judgments of data usage based on the data quality. The purpose of step 1 is to calibrate the neutron logs scaled based on the limestone matrix to represent the porosity of different lithologic units described in section 1, or the porosity values that would occur in sandstone-shale inter-beds, cherty dolomite and dolomites. This involves the risk introduced by the descriptive matter of lithology for each litho-unit (rather than a percentage). Step 2 uses the core porosity measurements and the neutron porosity log from the Mississippian cherty dolomite reservoir as input (Dickman 4, a water injector) to derive a relationship for calibrating porosity logs in 18 wells over the entire target strata. This step involves the risk that only 37 feet of cores in the Mississippian carbonate reservoir in one well has corresponding neutron log measurements to derive such a relationship. Step 3 uses results from steps 1 and 2 to compute the porosity logs that can be used in the Property model, therefore with combined risks from the previous steps.

Step 4 evaluates the relationship between the vertical and horizontal permeability measurements of cores to see if the permeability can be considered as isotopic. For core measurements in 6 wells for the Mississippian Carbonate reservoir, the two permeability curves are roughly parallel with a difference of less than 20%. Therefore, a single permeability is derived from the computed core porosity logs for the property modeling (in step 5). Step 5 involves risks that the reservoir permeability may not be isotopic in formations with quantities of sandstone/shale inter-beds, such as in the Pennsylvanian Cherokee Group, and in carbonate reservoirs where fractures result in preferred permeability distribution, such as seen in one core in the Dickman 5 well. Step 6 uses results from steps 3 and 5 to compute the permeability for the property mode. The purpose of steps 7-9 is to use seismic impedance values to assist the propagation of permeability through the Osagian saline aquifer since there are only 4 porosity data points to compute the permeability.

At the end of this work flow, all porosity logs and the computed permeability logs are up-scaled based on the two grids described in the structure modeling section. Values are assigned to cells on well traces to serve as seeds for the petrophysical modeling. The simplest kricking method is used to propagate the properties, and no general trend is removed during the modeling. The modeling process resulted in porosity and permeability grids for the two structure frameworks used in the CMG history matching and the CO₂ injection models, respectively.

Porosity and permeability grids

The zone-averaged property grids for two target reservoirs are used for the history-matching model. Maps showing the Mississippian Carbonate reservoir thickness (from well top) layer-averaged porosity and computed permeability for the Mississippian porous limestone along with histograms of porosity and permeability distribution of the Mississippian carbonate reservoir have been created. The maps indicate that the high reservoir porosity (8-25%, averaging 21%) results in very low reservoir permeability (mostly below 40md, and no more than 70md). From core measurements, the reservoir core has a very high water saturation (35-70%). Therefore the conductivity of this high-porosity, low permeability carbonate reservoir must be enhanced by the presence of fractures, as seen in the pay zone of the Humphrey 4-18 well.

Similar maps and histograms for the Lower Cherokee sandstone reservoir have been created and show that the porosity for the Lower Cherokee Sandstone is slightly higher than that for the carbonate reservoir with a much higher permeability (up to 100 md). Because of the limited number of data points (only 3 producing wells), the modeling results for the Lower Cherokee Sandstone reservoir is not as reliable as those for the Mississippian carbonate reservoirs.

Figure 7 shows the porosity grid for the layer-averaged model viewed from east toward the Dickman Field, with a 5X vertical exaggeration. This is similar to the permeability grid. Layers from top to base are: Fort Scott Limestone, Cherokee Group (shallow reservoir not in focus of this study), Lower Cherokee Sandstone (sandstone reservoir), Mississippian to Osage (Mississippian carbonate reservoir), Osage to Gilmore City (the saline aquifer), and the saline aquifer below Gilmore City (not in focus of

history matching). The semi-transparent green surface is the oil water contact (OWC). The above property grids for the target reservoirs are extrapolated to the entire stratigraphic section for the CO₂ injection modeling.

The lack of scaled neutron porosity logs in the southwest corner of the rectangular grid reduced the accuracy of porosity and permeability in that area. Since it is an input data set to the CMG model, this in turn affects the precision of simulated reservoir conductivity in CMG models.

Discussions on the geological events and fault/fracture system

This section presents a summary on the local geological events and their effects on the reservoir conductivity. Details with maps will be discussed in the next report.

Major geological events

Figure 8 shows the plate tectonics during the Mississippian-Pennsylvanian deposition. The major geological events, the deposition of Middle-Upper Mississippian shelf carbonates; the exposure of Middle-Upper Mississippian Strata associated by karst-development; and deposition of Pennsylvanian Coal-bearing formations over the Mississippian Unconformity, were affected by the collision of the two continents to the south of the studied area, starting around 335Ma and ending around 310 Ma.

At a smaller time scale, the geological events of the studied area, from oldest to youngest, are summarized as the following.

1. Post-GilmoreCity (short term) exposure, associated with the early stage of karst development, typical of vertical erosion-dominated landscape concentrating on intersections of major NW and NE fractures, as sinkholes (shown by the curvature attribute) at the Gilmore City (GMC) unconformity.
2. Deposition of Osage strata on GMC as carbonate shelf, formation of litho facies that affect the distribution of primary porosity within strata, and the varying resistance to diagenesis, fracturing and erosion.
3. Exposure of Osage strata (shorter term), resulting in bedding-perpendicular and/or bedding-parallel fracture and/or pressure solution zones in the deep saline aquifer.

4. Deposition of Warsaw-Salem (maybe even younger) carbonate strata on shelf, formation of carbonate facies that affect the distribution of primary porosity of the reservoir and the varying resistance to diagenesis, fracturing, and erosion.
5. Post Mississippian (longer term) exposure of Salem/Warsaw, associated with mature stage karst development along planes of weakness (fractures), typical of horizontal erosion-dominated landscape, such as underground caves/tunnels and collapsed tunnels connecting relic sinkholes, resulting in fractured zones, pressure solution zones and karst breccia zones that favor the conductivity of the carbonate reservoir.
6. Deposition of Lower Cherokee Cherty Conglomerate and Sandstone within the relic channels (reservoir) on the Mississippian Unconformity, resulting in the sandstone reservoir.
7. Interwoven cyclic of carbonate shelf and coastal coal swamp facies, ending with the Fort Scott Limestone, as sealing layers.
8. Post-Pennsylvanian folding and fracturing to form a shallow NE 35-oriented fold perpendicular to the axis of CKU, formation of several 20-40 ft closures oriented in NE direction.
9. Post-Pennsylvanian faulting on the NW flank of the fold, both Mississippian and Pennsylvanian Fort Scott strata at the foot wall were lifted and tilted to SE, resulting in the seal NE Boundary Fault.

In additional to the major NE boundary faults, NE or NW oriented lineations (discontinuities) were revealed by various seismic attributes as described in the 2009 Q2 report. Most of them, including very low angle ones, are components of a local fault/fracture framework attributed to the activities along the basement lineation. The dendritic drainage system on surface suggests that this framework also controls the present day landscape.

Lineations and discontinuities in this framework can be classified as: 1. high angle planes parallel to the axis of CKU (older, NW-oriented) including bedding-perpendicular pressure-solution features; 2. high angle planes perpendicular to CKU (older and/or younger NE); 3. bedding-parallel planes (mostly revealed by ANT) including bed-parallel pressure-solution surfaces and solution seams that generally form

parallel to the depositional fabric following internal layering. The lineation patterns were smeared by karst development in different degrees near unconformities.

Geophysics

Progress made from the geophysical data include synthetic generation and quantitative evaluation with optimization near the seal of the reservoir and depth conversion of the Fort Scott Limestone formation. There are several ways to create synthetic logs from the available data within the Dickman field, which can lead to different depth conversion maps. Quantitative analysis is being conducted to ensure the best synthetic and the best depth conversion available is being used.

Synthetics

Synthetic logs can be used to correlate well logs to seismic data so that specific formations can be linked to specific reflections in the seismic data and mapped throughout the study area. They are also useful in correcting time-depth curves, which could then be used in depth conversion of mapped horizons. Since there are no checkshots within Dickman field, all the time-depth curves have been integrated from well logs. Most of the well logs in this field are noisy and restricted to specific depths and will only give approximate time-depth relationships. While synthetic seismic traces created from these logs may correlate well with the real seismic data, they could be shifted in time or relatively compressed or extended. Adjusting the synthetic to match the seismic will adjust the time-depth curve so that it will hopefully be more accurate.

A synthetic log is created by producing a reflection coefficient series from well log data and convolving the RC series with a wavelet. An RC series can be computed from a sonic or resistivity log alone or in conjunction with a density log. A wavelet can be extracted from the seismic data or approximated with a theoretical wavelet.

To test the reliability of the well logs available, a variety of synthetics were created from the 5 wells that have both sonic and density logs. Two of these logs also

have resistivity logs. Reflection coefficient series were made from the possible combinations of logs (sonic alone, sonic with density, resistivity alone, resistivity with density) were convolved with two different wavelets: a theoretical Ricker wavelet and a wavelet that has been extracted from the seismic data near the corresponding well. A script was written in MATLAB to compare each synthetic to a trace near the well. Figure 9 shows an example of the figure created in the script using a synthetic created from the sonic and density logs from the Humphrey 4-18 well. (a) shows the synthetic and real seismic traces. (b) shows the difference. (c) shows the cross correlation. (d) shows the correlation coefficients for a certain area. Once all the synthetic correlations have been calculated, the best synthetic can be chosen quantitatively.

Depth Conversion

The Fort Scott Limestone is considered to be the seal of the reservoir so analysis of this horizon is critical in understanding the storage capacity of the Dickman Field. A positive reflection was tracked throughout the survey that corresponds well to the Fort Scott formation tops. A flex grid with an 82.5 ft grid size was applied with a residual fit to the data with minimum curvature and heavy smoothness.

One method to depth convert a horizon is by using a time-depth curve. There are several different time-depth curves available for the Dickman Field from several different wells, so depth maps were created for each of them. Figure 10 shows each of these depth horizons. The black circle indicates the location of the time-depth curve that was used for each map.

To quantify which time-depth curve does the best job converting to depth relative to formation tops, a depth map was also created from the formation tops. A flex grid was used with similar parameters as the horizon grid except the bin size was increased to 500ft. The map is given in Figure 11, with wells shown that were included in the grid computation. To quantify which time-depth curve did the best job converting to depth relative to formation tops, each horizon depth map was subtracted from the from the formation top grid. Figure 12 shows the resulting maps. A colorbar was chosen so that areas of no color indicate a good fit to the formation tops and areas with color indicate a

poorer fit. Typically, the maps fit well in areas near horizon tops and in the area around the well containing the used time-depth curve.

Acoustic Inversion

There are six wells with sonic curves in the Dickman field, each of which penetrate just below the top of the Mississippian. For inversion to be feasible, input well data must be within the 3D seismic survey boundary so only data from the Elmore 3 and Dickman 6 wells were used. Two time-depth tables generated from these wells, four horizons which vary from shallow to deep on the section, Mississippian and Fort Scott well tops, and a wavelet extracted from the time interval from the target zone (800-900ms) were used as input into Hampson-Russel software to perform poststack acoustic impedance inversion on the full stack seismic volume.

Figures 13 and 14 show the inversion result in the inline and crossline directions respectively. The upper left corner of these figures show a time structure map for the top of the Mississippian and the location of the displayed seismic line. The sonic curve is displayed with the time-depth function applied.

The color bar indicates different impedance contrasts which are directly tied to the geology. Since the inversion result relies mostly on the seismic data, useful information is provided in areas with insufficient well control. This information can help validate the current geological model. According to the stratigraphy, the top of the Mississippian unconformity is mainly Cherokee Sandstone overlying Warsaw Limestone and Osage Limestone.

Figure 14B illustrates progress we have made in tuning the SPICE attribute (Li and Liner, 2008) for use in reservoir assessment for CO₂ sequestration. The large chair display in the figure is a SPICE volume computed from the seismic amplitude data. The small insert cube is seismic amplitude data. Note the improved resolution and delineation of geologic bedforms. The amplitude data cube rests approximately on the Mississippian unconformity, and the incised channel discussed elsewhere is clearly visible in the SPICE timeslice.

Time-lapse Seismic Modeling

This study will employ time-lapse seismic (4D) to monitor the state of the reservoir, due to changes of fluid properties at periodic times. The fluid properties, which include a number of parameters such as porosity, saturation, permeability, pressure, temperature, etc. will have impact on the seismic responses. Hence, by differencing the seismic responses at varied times the reservoir characteristics can be analyzed.

The current CO₂ flow simulation calculations and Gassmann's theory can be used for the fluid substitutions. The link between rock physics and seismic modeling is realized by first calculating the seismic velocity and density for the saturated rock at each simulation cell, then calculating seismic reflection coefficients from impedance contrast. Given an input wavelet, seismograms can be generated by some modeling method. A few good candidates can be the modest convolutional model, ray-tracing using Eikonal solver and two-way wave modeling by finite difference.

The simulation output can be considered as a three-dimensional volume with the size of $\mathbf{M} \times \mathbf{N} \times \mathbf{L}$ in x, y, z directions, as illustrated in Figure 15. The seismic bin size is defined as that of the simulation cell bin size. In each bin, the seismic synthetics are generated as a summed trace. For each grid within the seismic bin, all the parameters from the simulation output are read to calculate impedance, and then the reflection coefficients are calculated.

Below is a 2D case as an example. As illustrated in Figure 16, for the j th simulation column within the seismic bin ($j=1, \dots, M$), the time-lapse seismic modeling works as follows:

- Read the i th simulation grid ($i=1, \dots, N$), which contains the information of porosity, saturated density, pressure, water, gas and oil saturations, etc.
 - 1) Compute the bulk modulus for the porous rock frame. In this experiment we consider that the mineral is Quartz, so the mineral bulk modulus is known. The bulk modulus of the porous rock frame also has the relationship (Liner, 2004):

$$\left| K_{dry} = \frac{K_{min}}{a + b\phi^c} \right|$$

K_{min} is the bulk modulus for the mineral, and a, b and c are the coefficients to be determined.

2) Compute bulk modulus for different fluids (oil, gas, water, brine)

i. Bulk modulus for oil

The density of oil can be obtained by a series of equations which relate to the fluid gravity (G), reservoir temperature (T), and fluid pressure (P) as below (Batzle and Wang, 1992):

$$\rho_{oil} = \rho_G + (0.00277 - P - 1.71 \times 10^{-7} P^3)(\rho_G - 1.15)^2 + 3.49 \times 10^{-4} P$$

$$\rho_G = (\rho_o + 0.002GR_G)/B_o$$

$$\rho_o = \frac{141.5}{API + 131.5}$$

$$R_G = 3.03G(Pe^{0.02878API - 0.00377T}) \times 1.205$$

$$B_o = 0.972 + 0.00038 \times [2.4R_G \sqrt{\frac{G}{\rho_o}} + T + 17.8]^{1.175}$$

The velocity of oil can be calculated by (Batzle and Wang, 1992):

$$V_{oil} = 2096 \left(\frac{\rho'}{2.6 - \rho'} \right)^{0.5} - 3.7T + 4.64P + 0.015 \times [4.12 \sqrt{\frac{1.08}{\rho' - 1}}] TP$$

$$\rho' = \frac{\rho_o}{B_o(1 + 0.001R_G)}$$

Thus the bulk modulus for oil can be attained by (Batzle and Wang, 1992):

$$K_{oil} = \rho_{oil} V_{oil}^2 / 1000$$

ii. Bulk modulus for water:

$$K_w = 2.2 \times 10^9 pa$$

iii. Bulk modulus for gas. Since there is no gas in the field $K_g=0$

iv: Compute bulk modulus for saturated rock.

The fluid saturated density satisfies the relationship between the fluid density, grain density of the rock matrix and porosity:

$$\rho_{sat} = (1 - \phi)\rho_{min} + \phi\rho_{fluid}$$

$$\rho_{fluid} = S_w\rho_w + S_o\rho_{oil}$$

The total bulk modulus for the fluid is:

$$\frac{1}{K_{fluid}} = \frac{S_w}{K_w} + \frac{S_{oil}}{K_{oil}} + \frac{S_g}{K_g}$$

Bring K_{min} , K_{dry} , K_{fluid} into Gassmann's equation to get K_{sat} :

$$K_{sat} = K_{dry} + \frac{(1 - \frac{K_{dry}}{K_{min}})^2}{\frac{\phi}{K_{fluid}} + \frac{1-\phi}{K_{min}} - \frac{K_{dry}}{K_{min}^2}}$$

based on the assumption that the shear modulus of fluid saturated rock and porous dry rock frame are equal, so:

$$\mu_{sat} = \mu_{dry}$$

3) Compute the velocity for the saturated rock by:

$$V_{sat} = \sqrt{\frac{K_{sat} + \frac{4}{3}\mu_{sat}}{\rho_{sat}}}$$

4) Compute impedance with saturated density and velocity in this simulation grid:

$$Z_i = V_{sat}\rho_{sat}$$

- Read the next simulation grid, and repeat the steps above until all the impedance values have been calculated in this bin.
- Calculate the reflection coefficients in this bin:

$$R(i) = \frac{Z_{i+1} - Z_i}{Z_{i+1} + Z_i}$$

- Read the next bin, $j=j+1$, repeat the steps above.

The final output will be a 3D seismic cube that can be interpreted for trapping, movement, and leakage of CO₂.

Reservoir Simulation

For the past quarter, the work has been focused on the establishment of a reliable Dickman saline aquifer CO₂ sequestration simulation model. Based on the improved result from a latest reservoir modeling analysis, a simulation model with six geological units and twenty-four simulation layers was established. A simulation sensitivity study was conducted to determine the optimal grid cell size and the effectiveness of local grid refinement (LGR). The influence of CO₂ injection and boundary conditions on aquifer pressure were also studied.

Dickman Reservoir Model Description

Figure 17 shows the reservoir model which will be used to create the simulation grid for CO₂ sequestration simulation. The model consists of the following six geological formation units:

1. Fort Scott Limestone
2. Cherokee Group
3. Lower Cherokee Sandstone
4. Mississippian Unconformity (low porous carbonate layer)
5. Mississippian Porous Carbonate
6. Mississippian Osage and Gilmore City

Figure 18 shows a depth contour map at the top of the reservoir model. The model covers an area of 3 x 3 miles. The 3D survey boundary and the location of all 22 production wells are also displayed.

Dickman field is located at Ness county, Kansas. Like most of the oil fields in Kansas, the majority of the oil reserve is in the Mississippian carbonate zone. The saline aquifer under Dickman field is part of Western Interior Plains Aquifer and Ozark Plateaus Aquifer. These two aquifers comprise one of the largest regional-scale saline and freshwater aquifer systems in North America. Figure 19 shows the aquifer salinity

distribution in Kansas. The salinity varies from fresh water TDS (Total Dissolved Solid) < 10 000 ppm to TDS > 100 000 ppm. The salinity of the aquifer under Ness County is about 45 000 ppm. The other two needed properties are temperature and pressure.

According to Timothy et al (2008), the reservoir temperature for the Mississippian and the deep saline aquifer (Arbuckle group) can be calculated by the following correlations

1. For the Mississippian

$$T = 0.0131(\text{depth}) + 55^{\circ}\text{F} \quad (1)$$

2. For the deep saline aquifer (Arbuckle group)

$$T = 0.0142(\text{depth}) + 55^{\circ}\text{F} \quad (2)$$

The pressure gradient is 0.476 psi/ft for both the Mississippian and the saline aquifer.

Because we lack well log data in the deep saline aquifer, Mississippian Osage and Gilmore City are treated as the only units belonging to deep saline aquifer. We expanded the average thickness of the Mississippian Osage and Gilmore City unit from 20 feet to 200 feet and established a simulation model with 24 simulation layers as shown in Figure 20. On average, the thickness of each simulation layer is about 20 feet. Table 1 lists the assignment of simulation layers among different geological units. The permeability data for each simulation layer are not yet available, so the permeability value for each simulation layer is assumed. Table 1 lists the assumed permeability values.

Simulation Convergent Study

A simulation convergent study has been conducted to determine grid size sensitivity for the Dickman Field. The single well CO₂ injection model shown in Figure 20 was used with the grid size varying from 1944 cells (9 x 9 x 24) to 285144 cells (109 x 109 x 24). Injection of CO₂ is simulated for the first 25 years and the injector was shutin thereafter. Table 2 is a summary of related parameters and reservoir properties used in the simulation convergent study. The relative permeability curves for brine/CO₂ are shown in Figure 21.

Analysis of several simulation run results indicated that total CO₂ dissolved in water was sensitive to grid cell size. Therefore we can use it as an accuracy indicator in

the convergence study. For simplicity, the residual CO₂ saturation in Table 2 was set as zero to exclude the influence of the residual CO₂ trapping effect.

The ratios of total amount of CO₂ dissolved into water to the total amount of CO₂ injected at 250 years were compared for different sizes of grids. CMG GEM simulator was used to perform the simulation for two types of grids: a uniform mesh grid and a grid with local grid refinement (LGR) applied around the injector borehole (Figure 22). As shown in Figure 22, the solution for dissolved CO₂ ratio converges to 11.5% asymptotically. The solution for a grid with about 95K cells (63 x 63 x 24) is 13.6% and has a corresponding grid cell size of 250 x 250 ft. To insure a simulation error under 20%, a grid cell size less than 250 feet is recommended. Figure 22 also indicates that applying LGR around the injector borehole can produce a more accurate simulation result with fewer simulation grid cells. For example, a 36K grid (39 x 39 x 24) allows use of a 400 ft cell while applying LGR around the borehole to reduce the simulation error from 40% to 20%.

It is inevitable that CO₂ injection will increase the reservoir pressure. High enough reservoir pressure will cause the formation to fracture, breaking the reservoir seal and leaking CO₂ back to the atmosphere. It is important to predict the reservoir pressure precisely during CO₂ injection. The aquifer model considered in this study is not an isolated aquifer. It is a part of a huge aquifer system (Western Interior Plains Aquifer and Ozark Plateaus Aquifer system) so proper boundary conditions must be applied to the simulation model in order to predict the reservoir pressure correctly. The conventional Carty-Tracy infinite extent aquifer boundary condition was used in this study. Figure 23 is a comparison of the aquifer pressure distribution at the initial state, the end of the injection, and the end of simulation. As shown in Figure 23, the maximum reservoir pressure varies from about 2000 psi to 2065 psi at 25 years (the end of CO₂ injection). At 250 years, the aquifer pressure distribution is almost the same as the initial pressure distribution. We will continue to study the pressure issue in relation to fracture gradient of the reservoir rocks.

Work Plan for the Next Quarter

Geology

As we approach completion of the project, geological efforts will be focused on gathering, organizing, and coordinating all geological information that has been developed during the project. This will be distilled in to a major section of the project final report.

Any additional geological information needed by the flow simulation, seismic interpretation, or inversion efforts will also be contributed as needed.

Geophysics

The MATLAB script for comparing synthetics to the seismic data needs to be modified so that the traces are normalized for more accurate correlation. Once this is completed, all of the synthetics can be compared to nearby seismic data for evaluation. The best synthetic can be manually stretched and squeezed in order to produce a more accurate fit. Changing the synthetic will adjust the time-depth curve so that it will be more accurate which we expect to produce a more accurate depth map. Once a more accurate depth map is created, evaluation of the seal of the reservoir through seismic attribute analysis can be conducted.

The next step for the acoustic impedance inversion will be to add the sonic log data from the Dickman 1 well as well as all available neutron and porosity logs, which will be an addition to the existing porosity distribution for the field.

Work will also continue on the fluid substitution work flow.

Reservoir Simulation

As indicated by Sifuetes et al (2009), the horizontal permeability is the most influential parameter on the total amount of CO₂ dissolved, as it facilitates the lateral migration of CO₂, enhancing dissolution into the brine. A true and accurate permeability property data are important for the accuracy of the simulation prediction. The work of

obtaining a set of true permeability data is underway. We plan to perform a series of CO₂ injection simulations and history matching when the permeability data are available. At present, the sensitivity study was only performed to the grid cell size. For the next quarter, a series of sensitivity studies will be applied to different reservoir properties such as horizontal permeability, salinity and etc. We will also test the effectiveness of using a horizontal well for CO₂ injection. Nghiem et al, (2009) indicated that injecting CO₂ with brine water can significantly increase CO₂ solubility. We will also test the effectiveness of this process.

Cost and Milestone Status

Baseline Costs Compared to Actual Incurred Costs

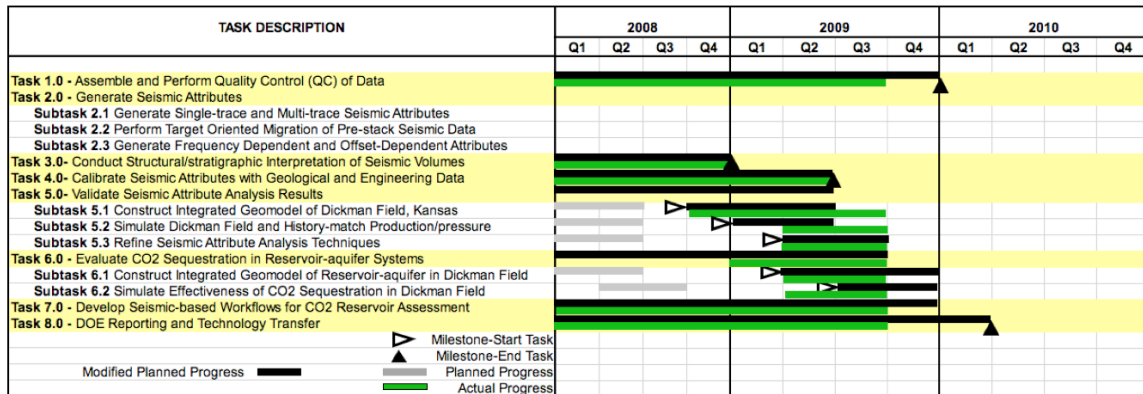
2009			
July 1 – Sept 30	Plan	Costs	Difference Plan minus Costs
Federal	\$25,000	\$25,027	(\$27)
Non-Federal	\$9,410	\$0	\$9,410
Total	\$34,910	\$25,027	\$9,883

Forecasted cash needs vs. actual incurred costs

Notes:

1. Federal plan amount based on original award of \$400K averaged over 12 reporting quarters.
2. Cost this period reflects 3 months salary for J. Zeng and P. Geng, and 1 month for H. King
3. Non-Federal plan amount based on original budget cost share of \$150,573 averaged as above.

Actual Progress Compared to Milestones



Note: Project years 1 and 2 (2006-7) not shown, and chart extended into 2010 in anticipation of no-cost project extension.

Summary of Significant Events

Problems and Significant Events

No problems to report.

As indicated in the Gantt chart above, we plan to request a 3 month no-cost extension of this project to 3/31/2010 to allow continued payment of Dr. June Zeng during the final report writing period.

The \$1.77M Dickman II DOE proposal (DE-FOA-0000023) was declined. The \$300K Dickman Training DOE proposal (DE-FOA-0000023) was funded, will support two students in training, and run for two years (1/1/2010 – 12/31/2011). This will continue work at Dickman on elastic modeling (industry partner: Geokinetics) in anticipation of future a proposal to acquire multicomponent 3D seismic data ideally suited to the purpose of CO₂ sequestration (rather than off-the-shelf petroleum seismic surveys). The new project will also continue work on attributes (industry partner: Fairfield).

Continuing Personnel

Prof. Christopher Liner is Principle Investigator and lead geophysicist. He is a member of the SEG CO₂ Committee, Associate Director of the Allied Geophysical Lab, and has been selected to deliver the 2012 SEG Distinguished Instructor Short Course.

Dr. Jianjun (June) Zeng has been working exclusively on this project since Dec 2007 and is lead geologist. She will be funded through the end of 2009.

Heather King is a graduate MS student in geophysics who joined the project in January 2009 as a research assistant. She will be funded out of the project Jan-May and Sept-Dec 2009, when she anticipates graduating. Her thesis will focus on Fort Scott to

demonstrate the integrity of this formation as a seal for injected CO₂. This will involve subtle structure and stratigraphy inferred by interpretation of multiple seismic attributes.

Dr. Po Geng has been working on this project as a specialist consultant since February, 2009. He will be funded out of the project, considered part-time, through the end of 2009.

Jintan Li is a graduate PhD student in geophysics who joined the project in Aug 2009. Due to budget limits, she is not funded on the project but we are actively seeking funding for her. Her thesis will be time-lapse seismic modeling (4D) for conducting dynamic reservoir characterization of the Dickman Field.

Technology Transfer Activities

There are no technology transfer activities to report this quarter.

Contributors

Christopher Liner (P.I, Geophysics)

Jianjun (June) Zeng (Geology and Petrel Modeling)

Po Geng (Flow Simulation)

Heather King (Geology and Geophysics, MS Candidate)

Jintan Li (Geology and Geophysics, Ph.D Candidate)

Tables

Sim Layer No.	Perm (md)	Formation Name
1 & 2	20	Ford Scott Limestone
3,4 & 5	30	Cherokee
6 & 7	100	Lower Cherokee
8	10	Mississippian Unconformity
9,10,11 & 12	150	Mississippian Porous Carbonate
13 - 24	20	Mississippian Osage & Gilmore City

Table 1. The distribution of 24 simulation layers among different geological layers and the permeability for each simulation layer

Parameter Name	Values	Unit
Reservoir Reference Depth (Subsea)	2000	feet
Reservoir Reference Depth (TVD)	4600	feet
Reservoir Reference Pressure	2190	psi
Reservoir Reference Temperature	121	F
Rock Compressibility	4E-6	1/psi
Water Salinity (TDS)	45,000	ppm
Residual CO ₂ saturation	0	
Residual Water Saturation	0.16	

Table 2: Reservoir parameters and properties used in the simulation convergence study.

Figures

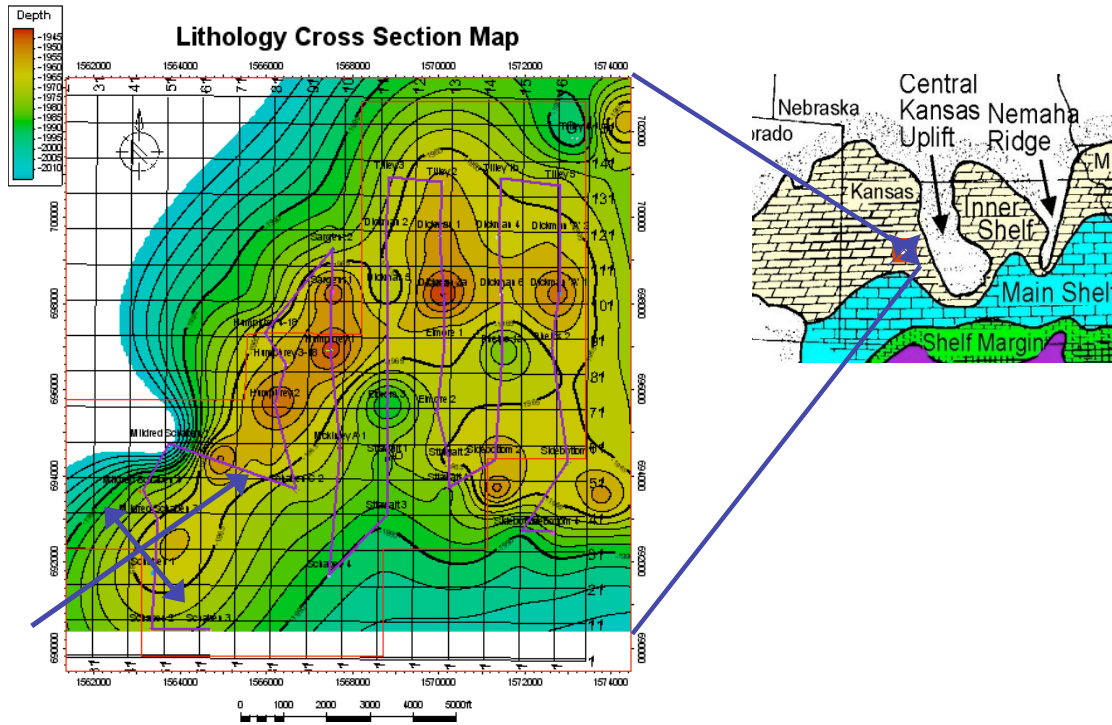


Figure 1: Cross sections (pink line) connecting wells with litho-zone logs. The section is also used for the seismic-well top ties during the time-depth conversion. The base map to upper-right is the top of Mississippian porous carbonate containing the reservoir. The blue arrows in southwest area indicate the fold.

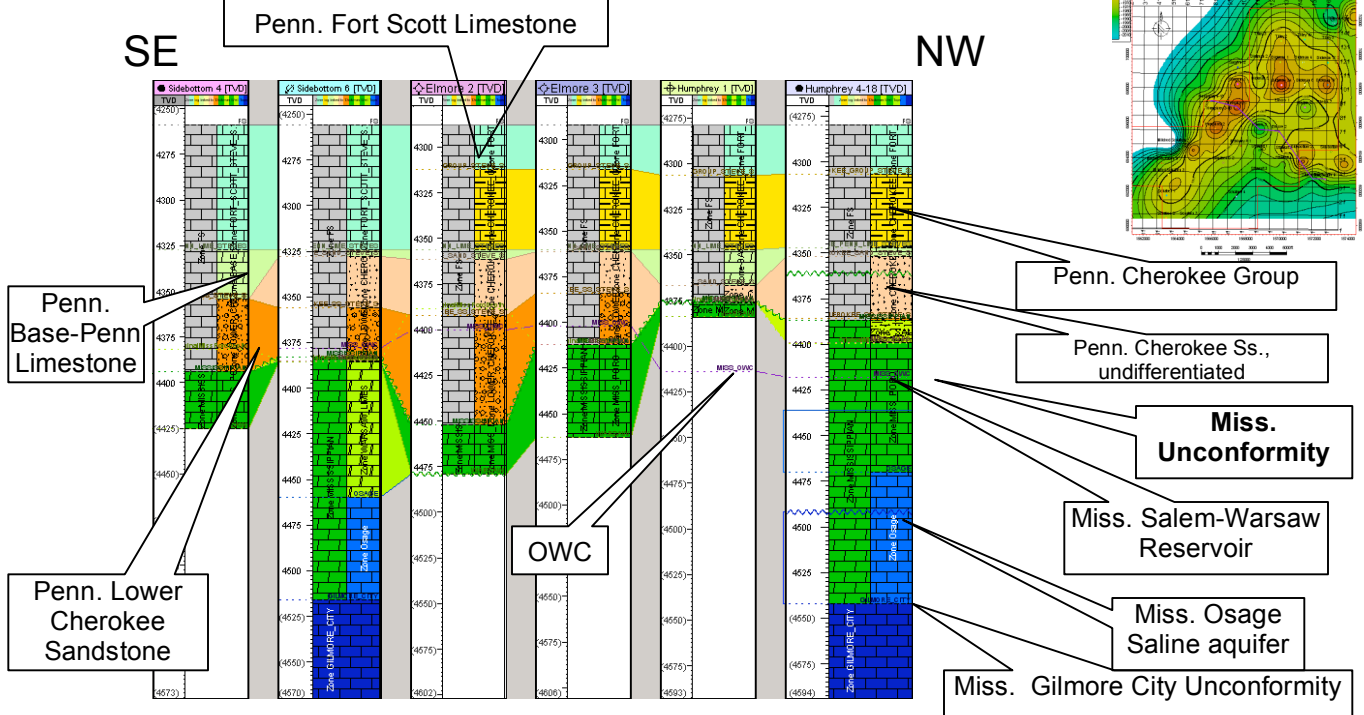


Figure 2: Lithologic cross section perpendicular to the axis of the structure across two topographic highs. Section is hung on Fort Scott Limestone top (same for the Figs.1-5b to 1-5e). One of the Mississippian lows are around the Elmore 2 with thickest Penn. Deposit. Purple line is the OWC.

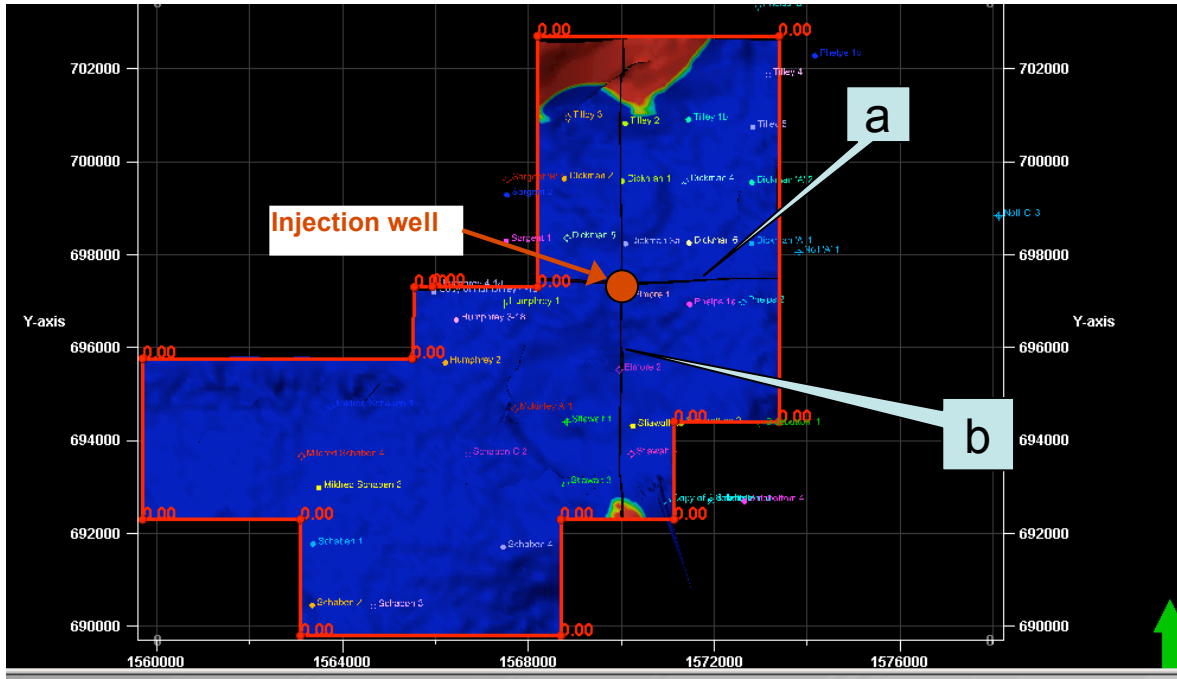


Figure 3: Center-lines of the CMG Flow Simulation Grid. a. E-W center line along Y=697500, b. N-S center line along X=1570000. Red dot: simulating CO₂ injector at 1570000 and 697500. One grid = 2000 ft.

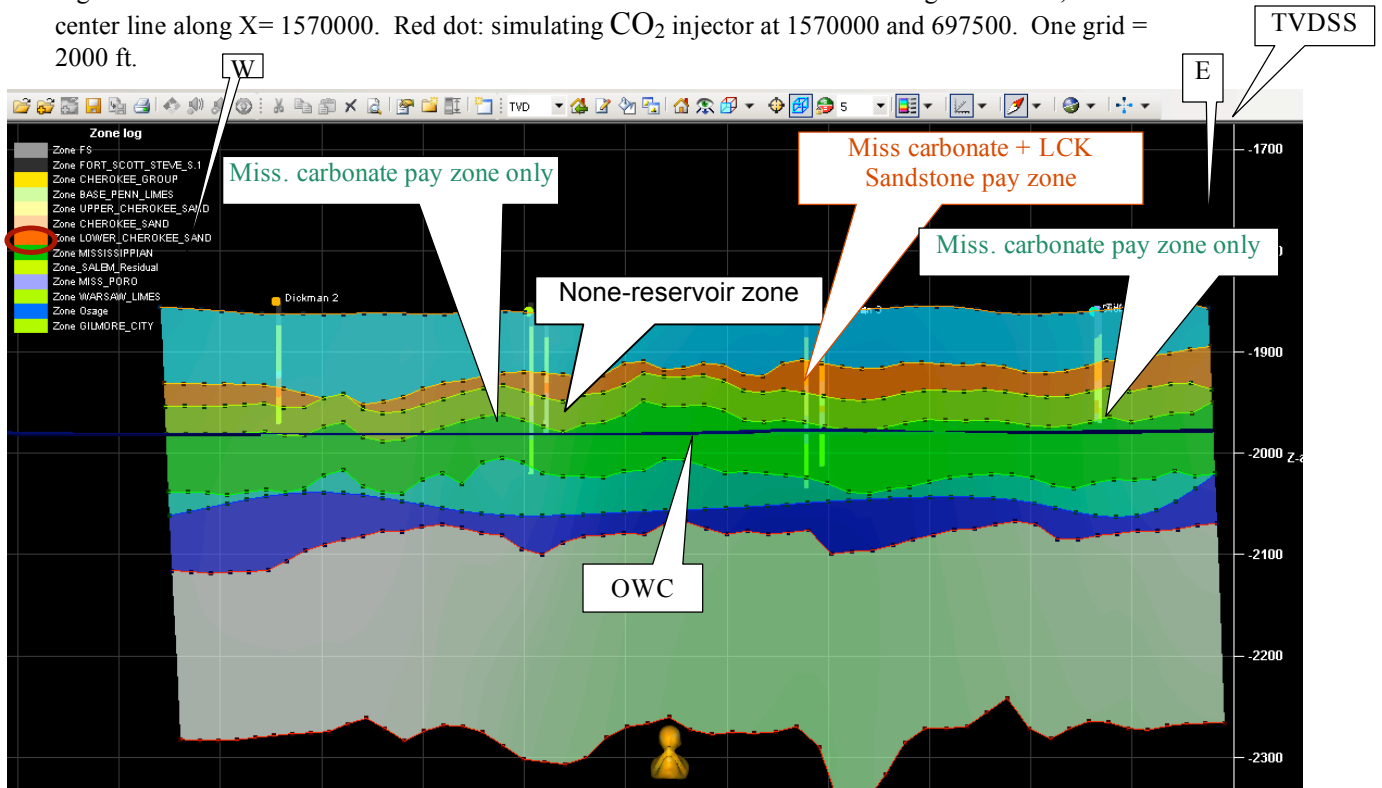


Figure 4: Well-control on the east-west center line of CMG model with wells, showing a good match between litho-zones (labeled in color bar) created from well tops (in depth domain) and litho-zones derived from geology-seismic combined model. The wells on this section did not penetrate the deep saline aquifer. The non-reservoir Miss. carbonate from the model is relatively thick compared with the zone logs (from well tops), probably due to the resolution of the seismic. One grid = 2000 ft.

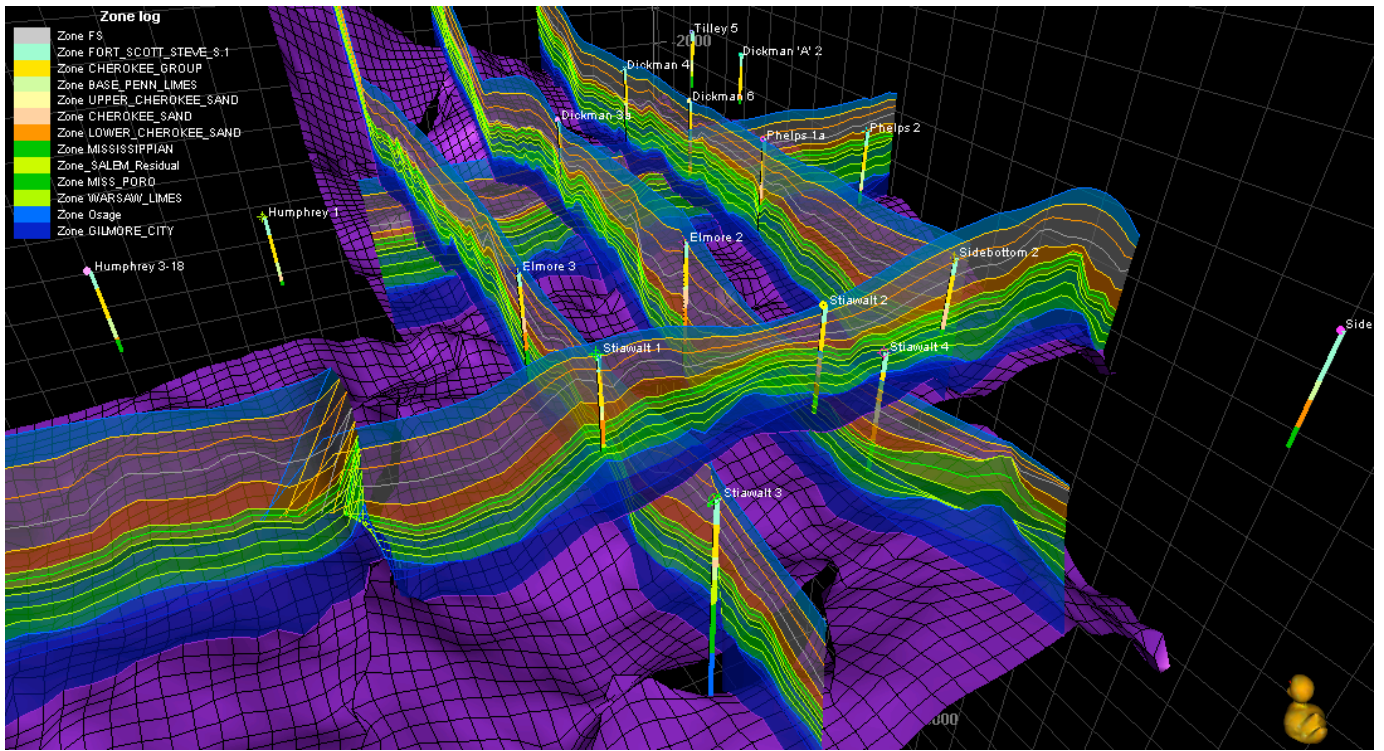


Figure 5: Well-control on the 16 layer CO₂ injection model. Base surface is the Gilmore City unconformity. The duck is facing north. Each layer in previous model is further divided in equal thickness sub-layers based on the analysis property distribution, to form a 16 layer model. The legend color is corresponding to the zone log color at each well-trace. Layering colors are assigned for better visualization.

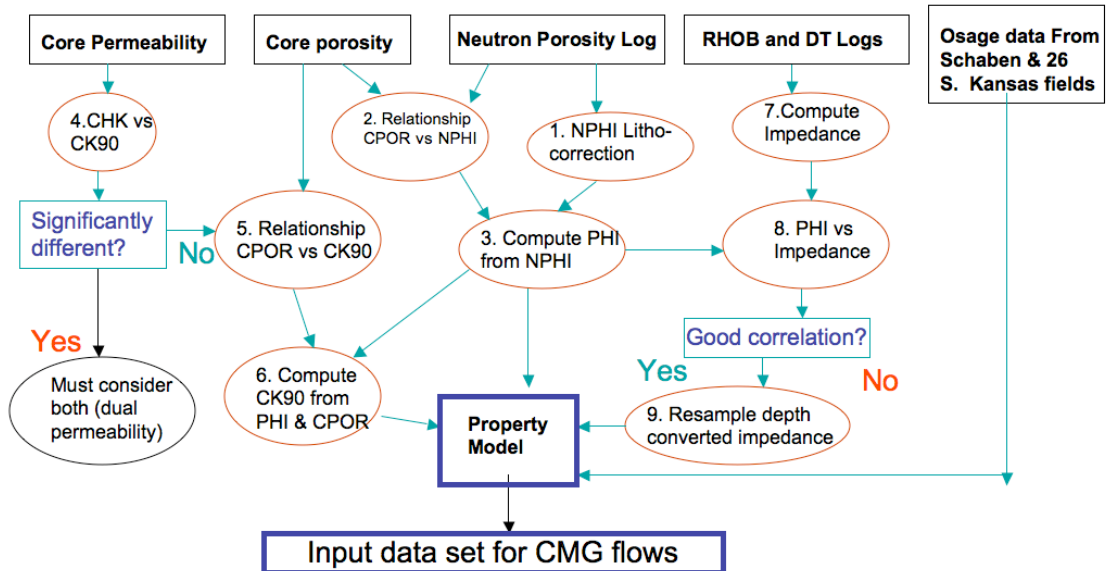


Figure 6: Work Flow Chart for Property Modeling Squares represent raw data, circles represent operations on data, arrows represent sets of data input to the operations and the direction of the work flow. Green color arrows following Yes or No is the direction we have gone in this project. Red circles: increasing risks in operation due to the poor data quality.

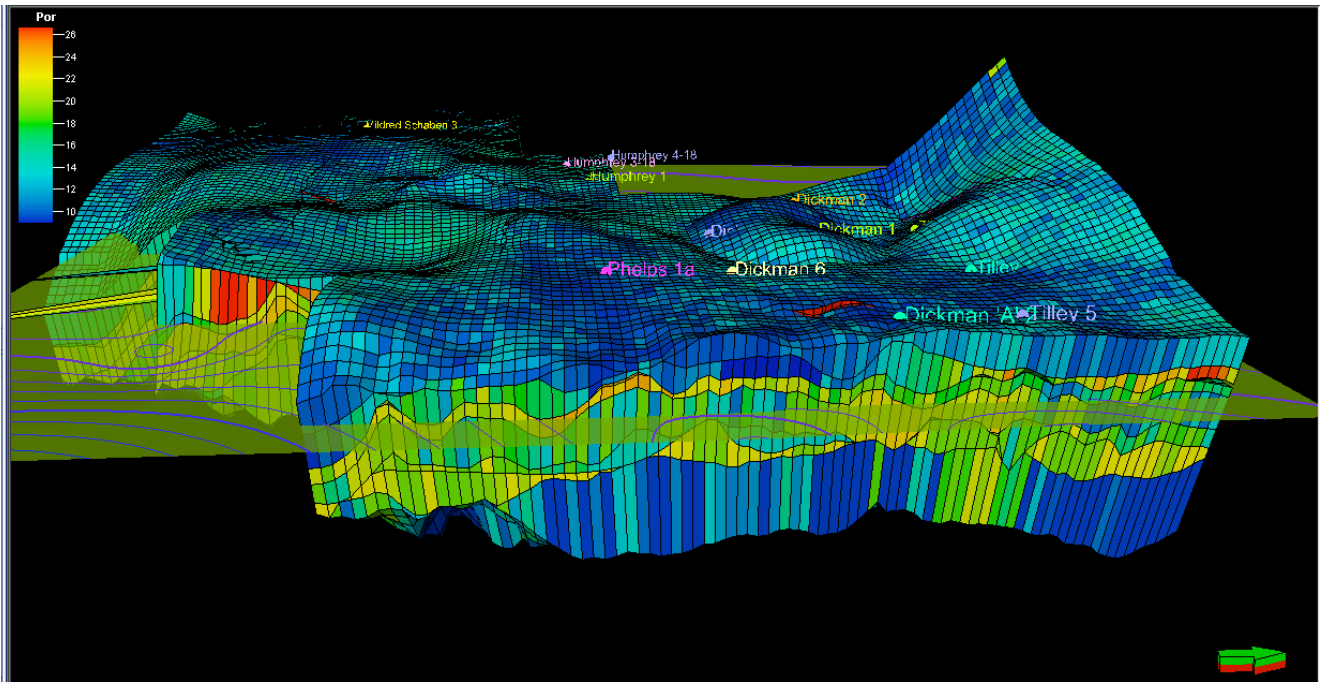
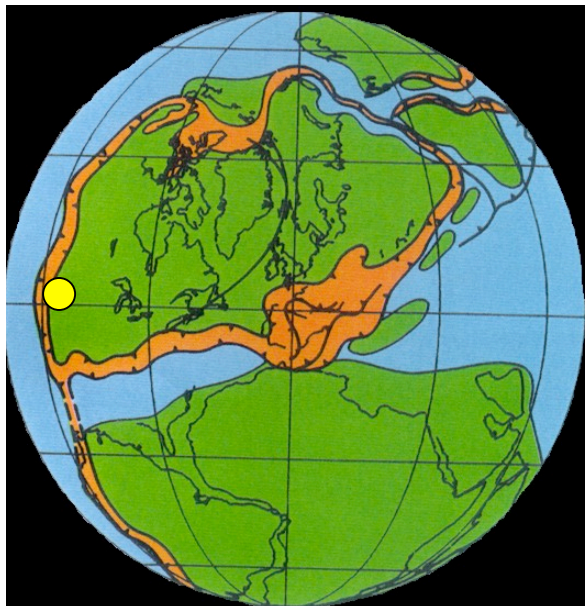
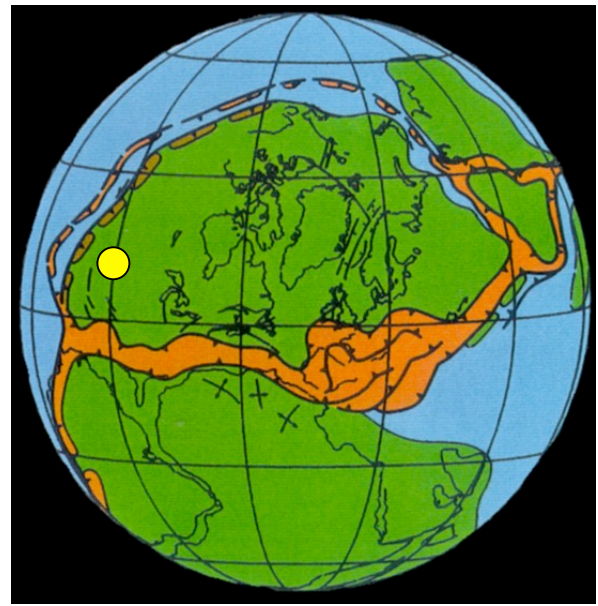


Figure 7: Porosity grid viewed from east toward the Dickman Field with 5X vertical exaggeration. Layers from top to base: Fort Scott Limestone, Cherokee Group (shallow reservoir not in focus of this study), Lower Cherokee Sandstone (sandstone reservoir), Miss. to Osage, containing the Miss. carbonate reservoir, Osage to Gilmore City the saline aquifer, and the saline aquifer below Gilmore City (not in focus of this study). The semi-transparent green surface is the OWC.



335 Ma Proto-Anadarko Basin
(Miss/Devo = 360Ma)



310 Ma Converging plates
(Penn/Miss = 320Ma)

Figure 8: Plate Tectonics During Carboniferous (after Zeigler, 1989)

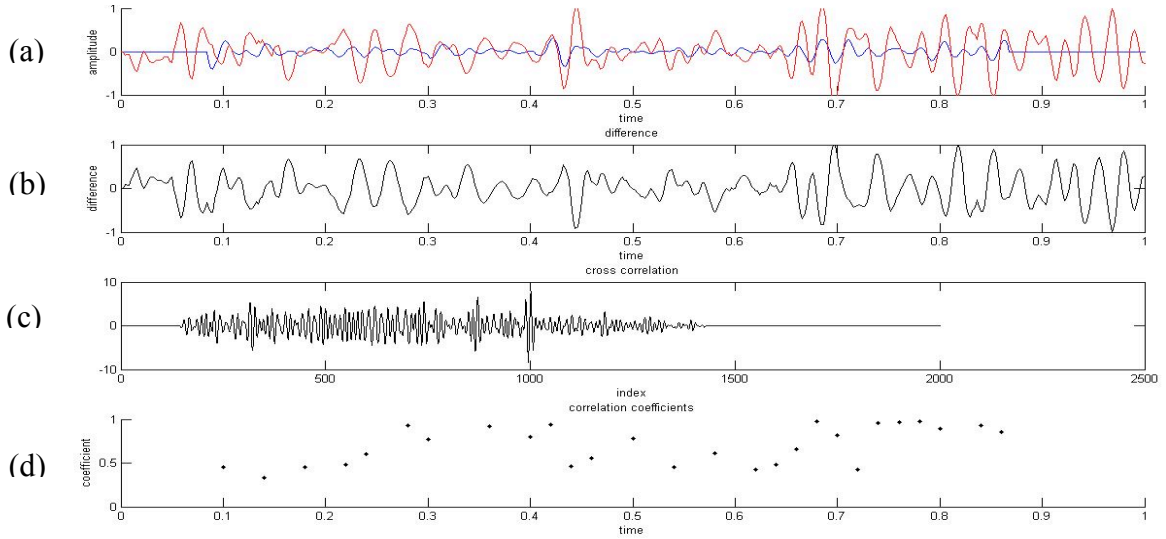


Figure 9: Comparison of a seismic trace near the Humphrey 4-18 well and a synthetic created from the sonic and density logs from that well. (a) shows the synthetic and real seismic traces. (b) shows the difference. (c) shows the cross correlation. (d) shows the correlation coefficients.

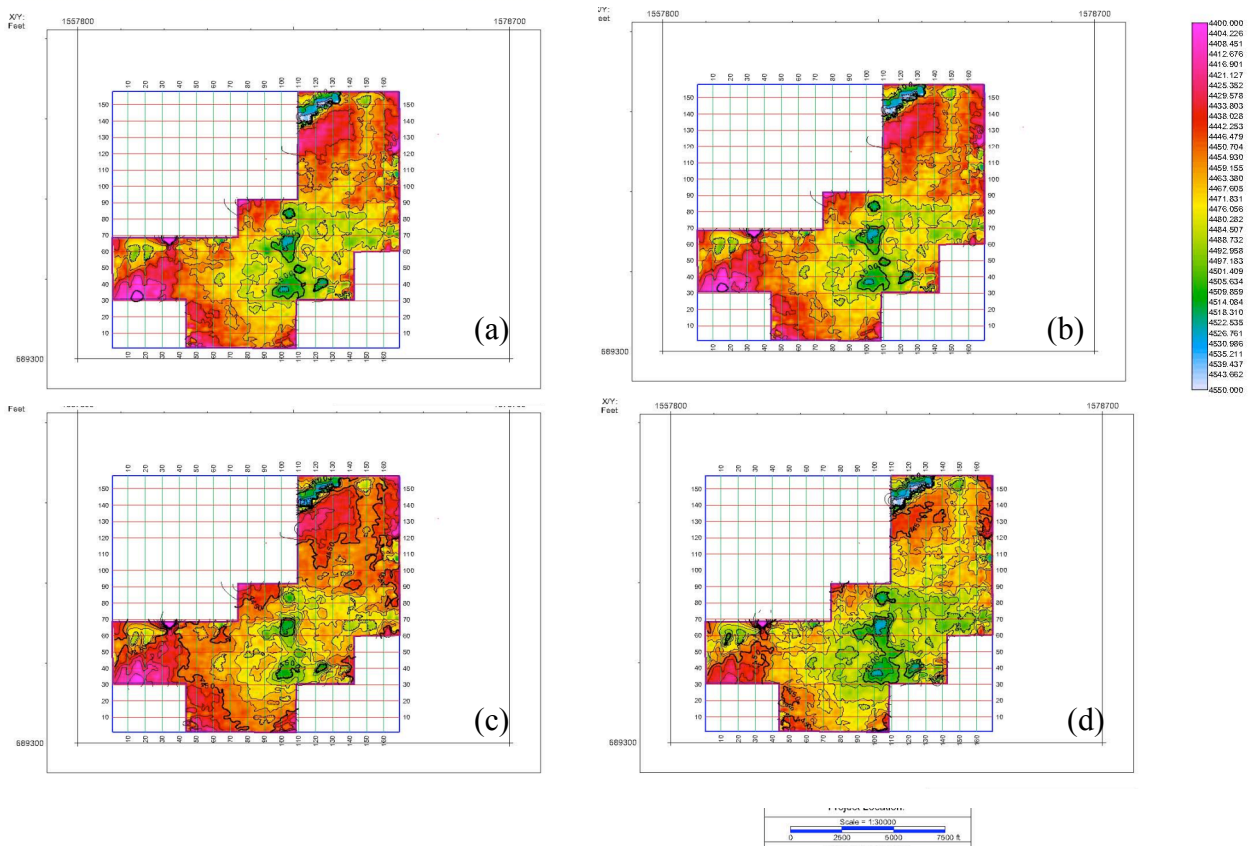


Figure 10: Fort Scott Horizon in Depth created from Time-Depth charts from wells (a) Elmore 3, (b) Schaben 4, (c) Sidebottom 6, and (d) Dickman 6.

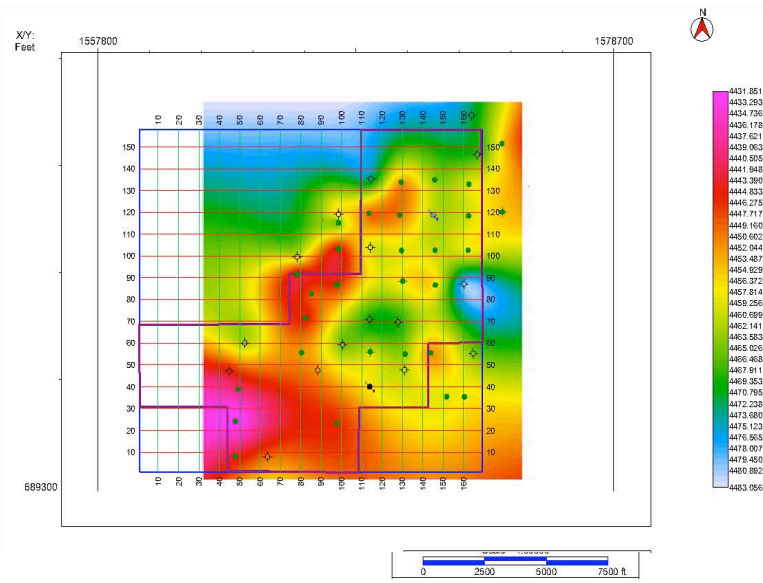


Figure 11: Fort Scott Horizon in Depth created from Formation Tops.

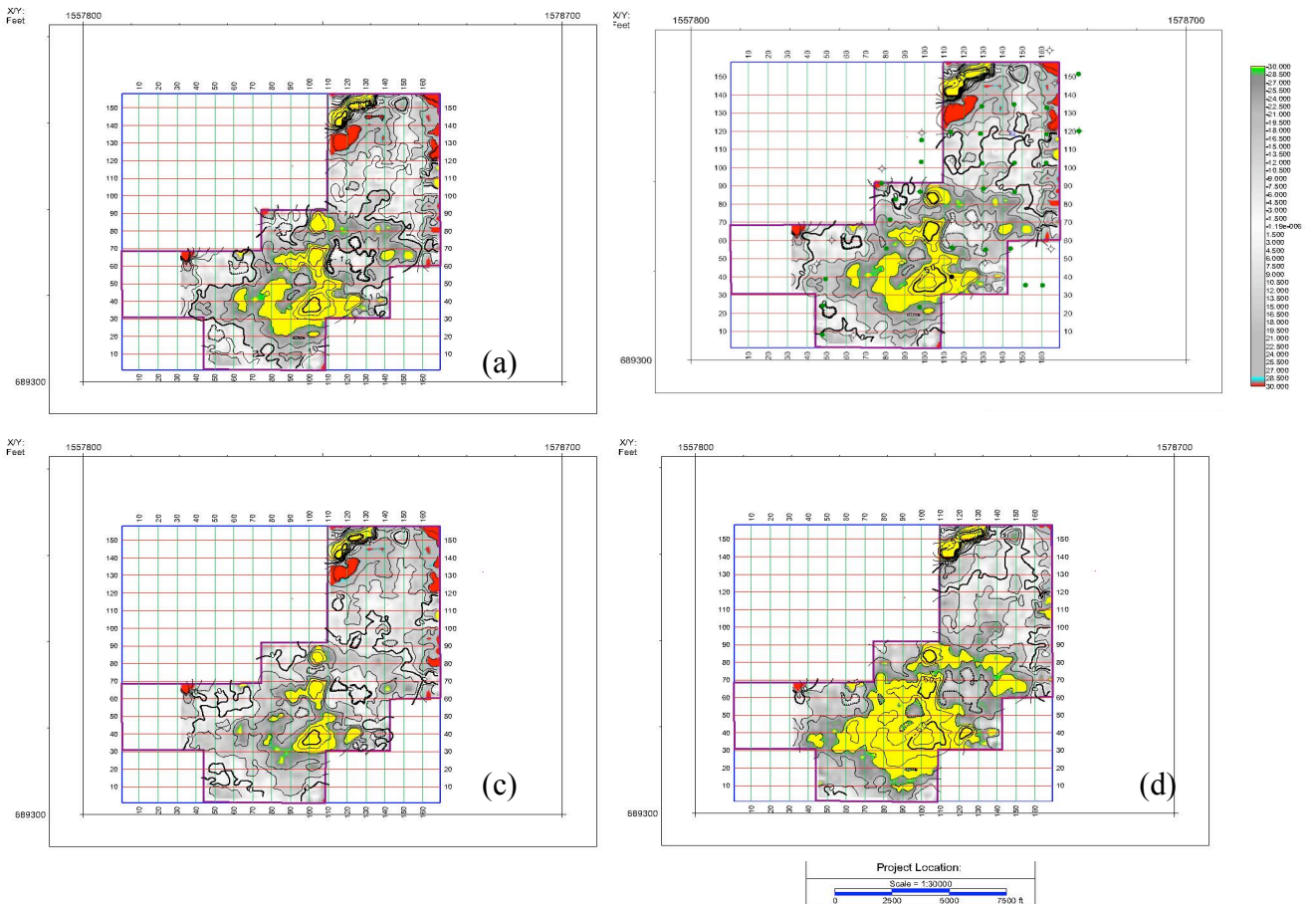


Figure 12: Fort Scott residuals created by subtracting the depth converted horizons from the formation top depth grid. Time-Depth charts used for depth conversion: (a) Elmore 3, (b) Schaben 4, (c) Sidebottom 6, and (d) Dickman 6.

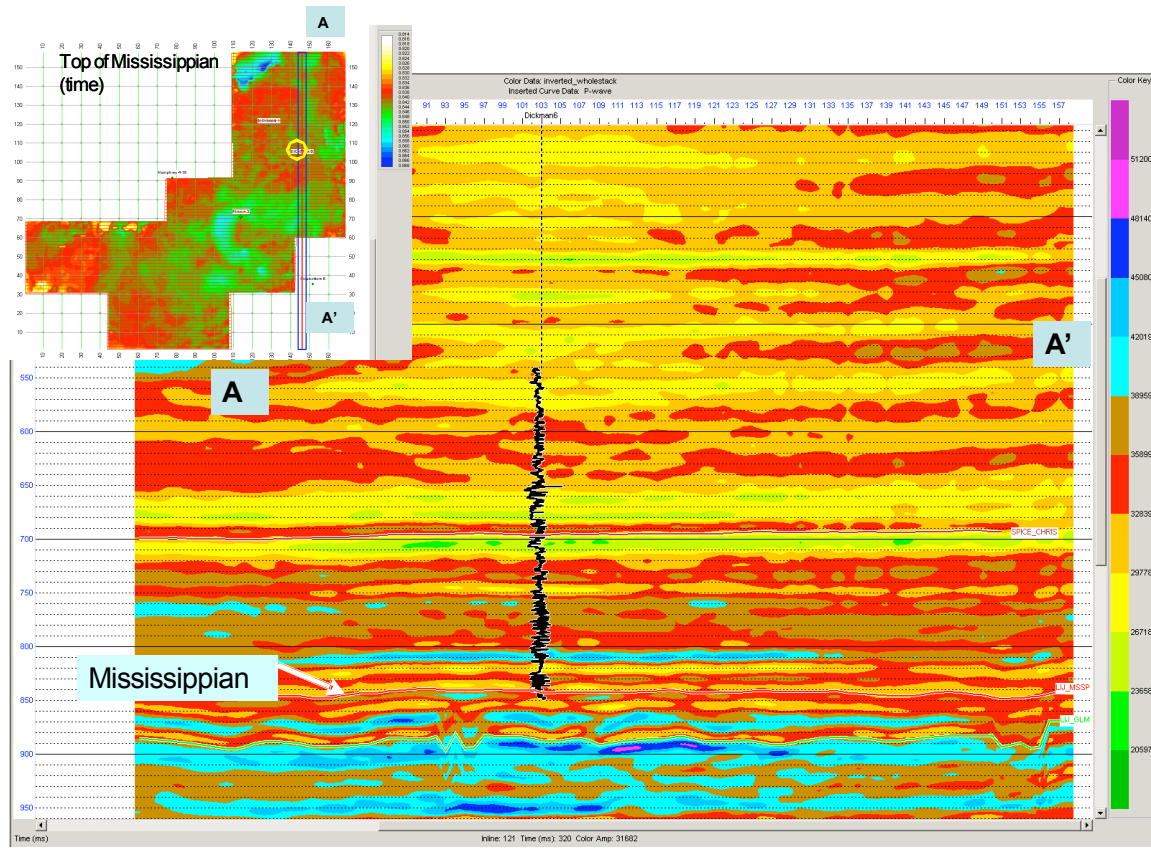


Figure 13: Inversion result for seismic line (crossline) including Dickman 6 well.

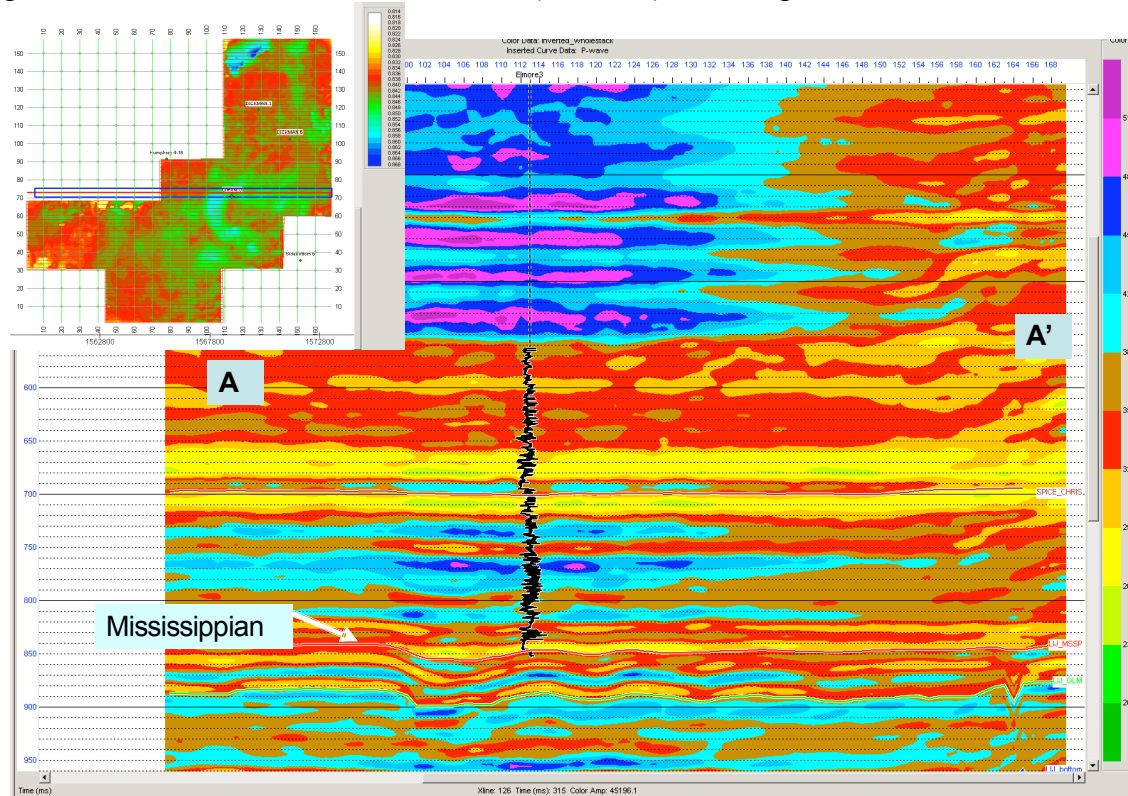


Figure 14: Inversion result for seismic line (inline) including Elmore 3 Well.

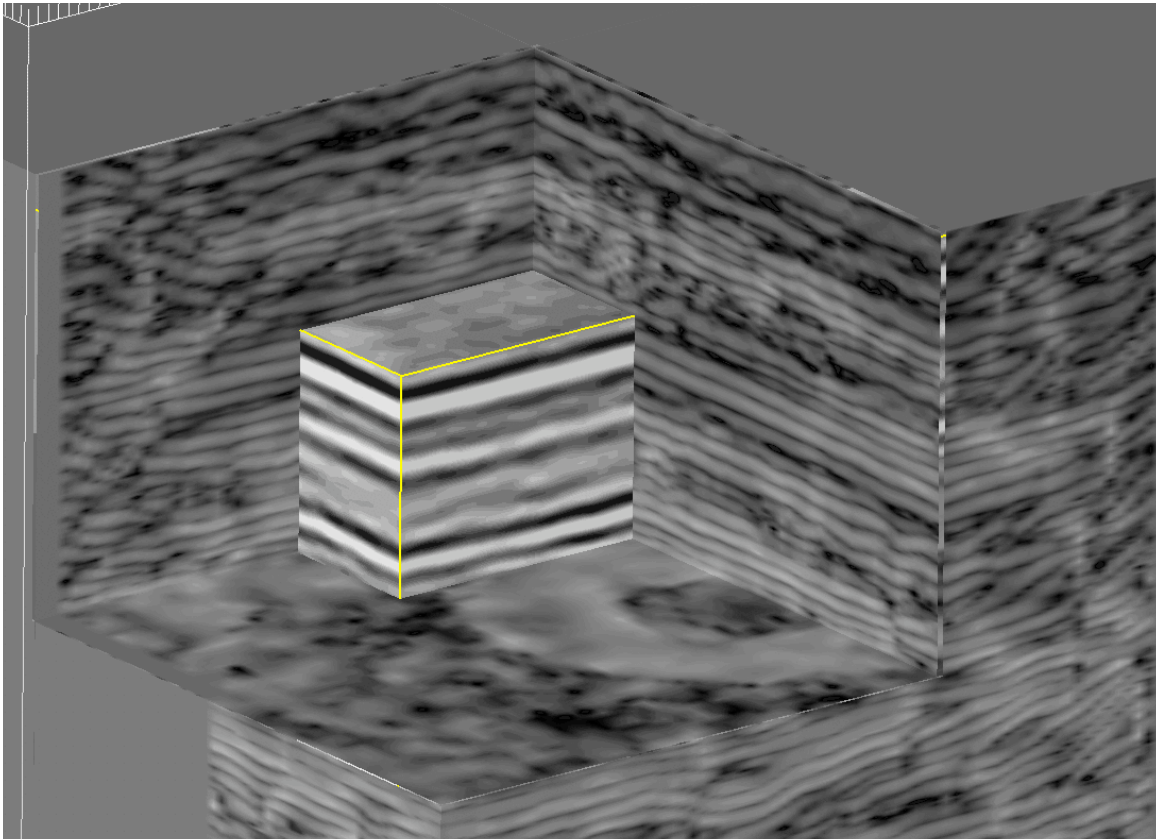


Figure 14B: Chair display of SPICE attribute volume co-rendered with a small cube of seismic amplitude data to illustrate improved resolution and delineation of geologic bedforms. Base of the amplitude cube rests at about 844 ms, coincident with incised channel at the top Mississippian. As seen on the far right front face of the SPICE cube, this attribute (like others) cannot distinguish seismic noise events from geological features. In this case, the events are edge effects near the boundary of the 3D data area. Away from edges, however, we believe SPICE can give geological information that cannot be interpreted by seismic amplitude data alone.

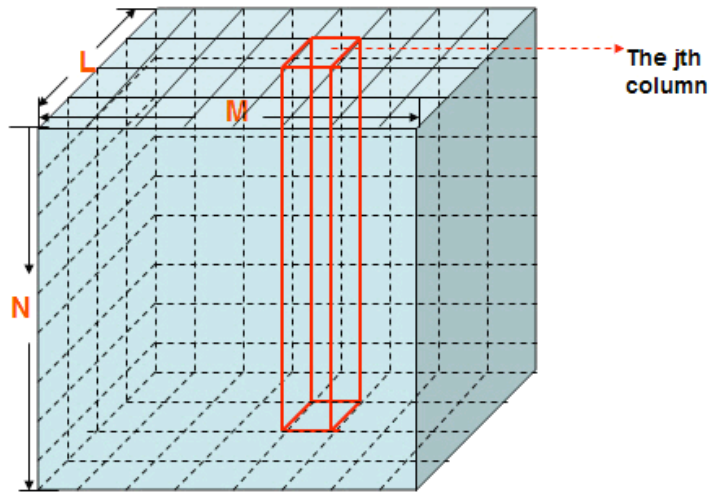


Figure 15: Flow Simulation 3D volume.

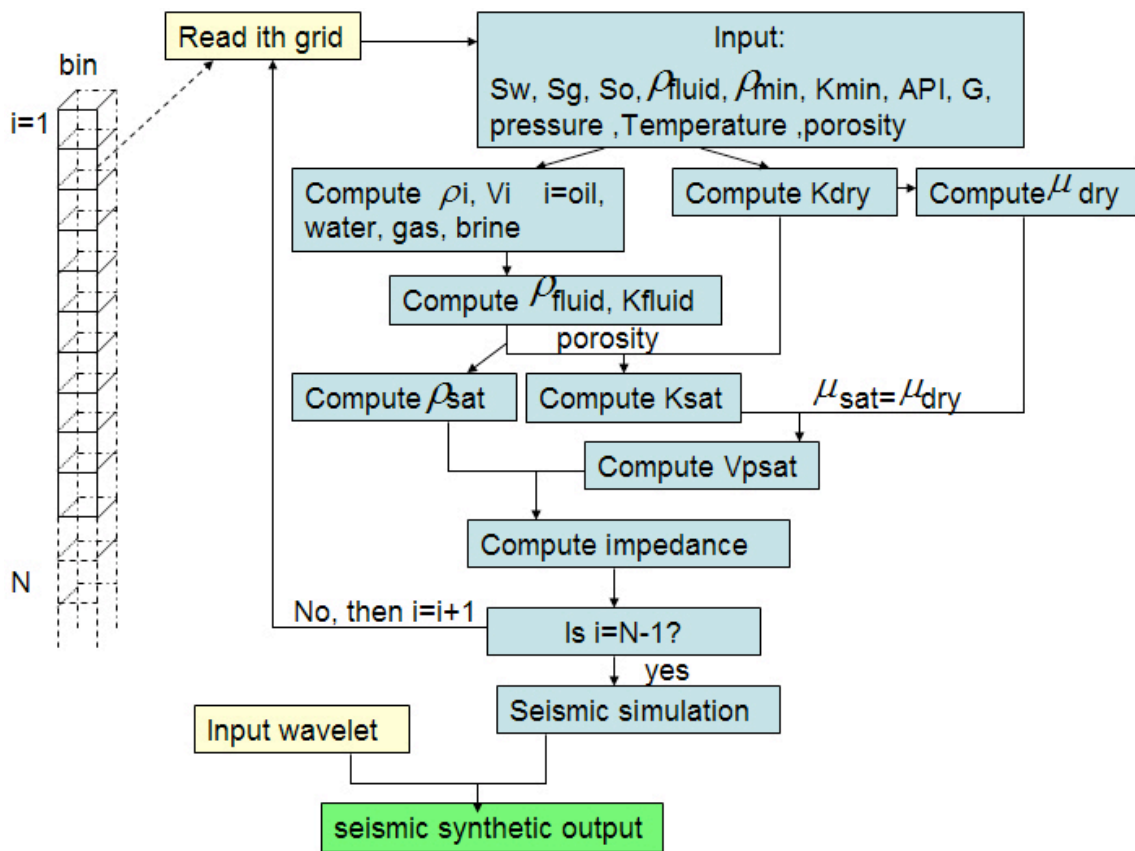


Figure 16: Time-lapse seismic modeling work flow for one simulation column.

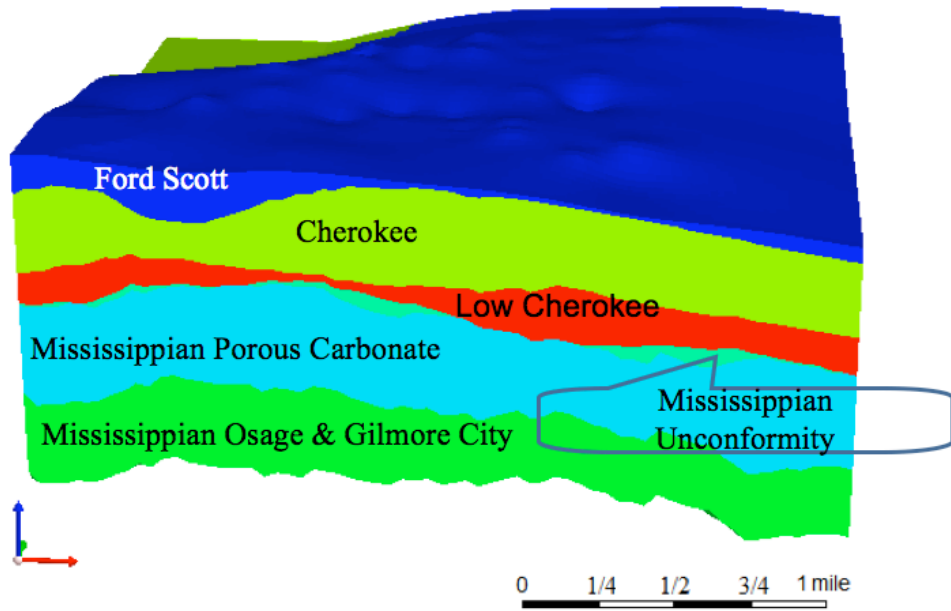


Figure 17: Reservoir model used for Dickman CO₂ sequestration simulation

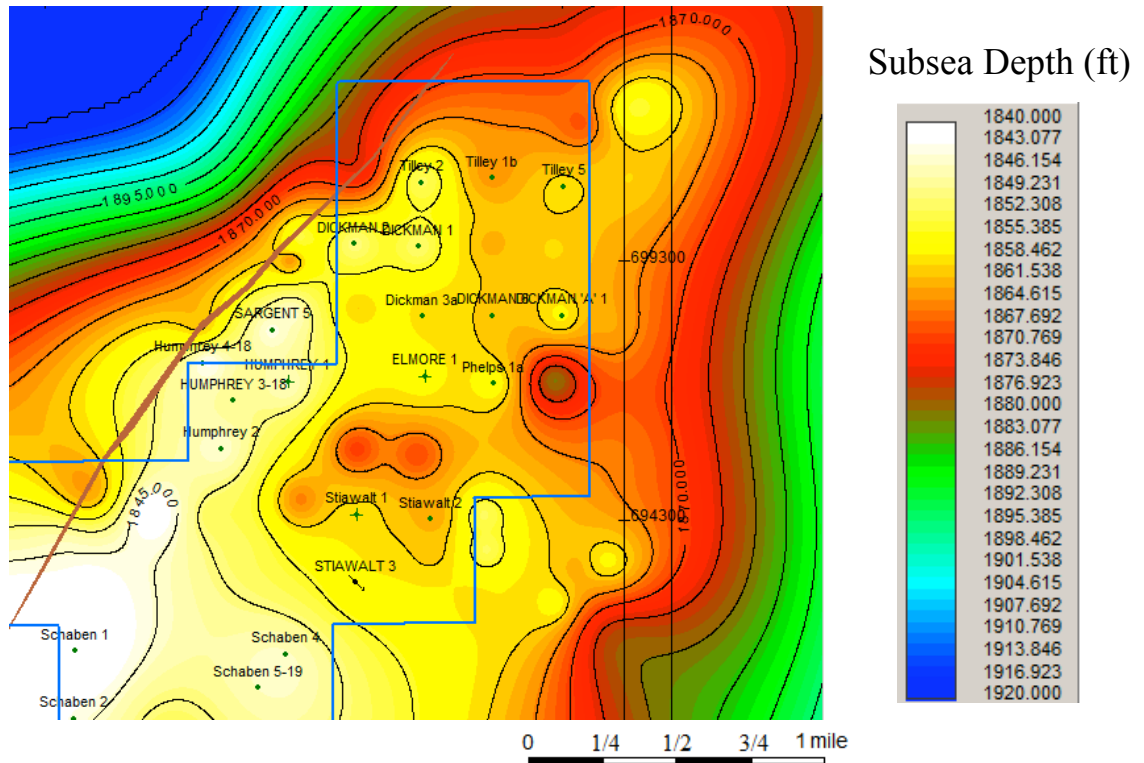


Figure 18: Top map view of Fort Scott Limestone unit. The locations of all 22 Dickman production wells are displayed and the blue lines are 3D survey boundaries.

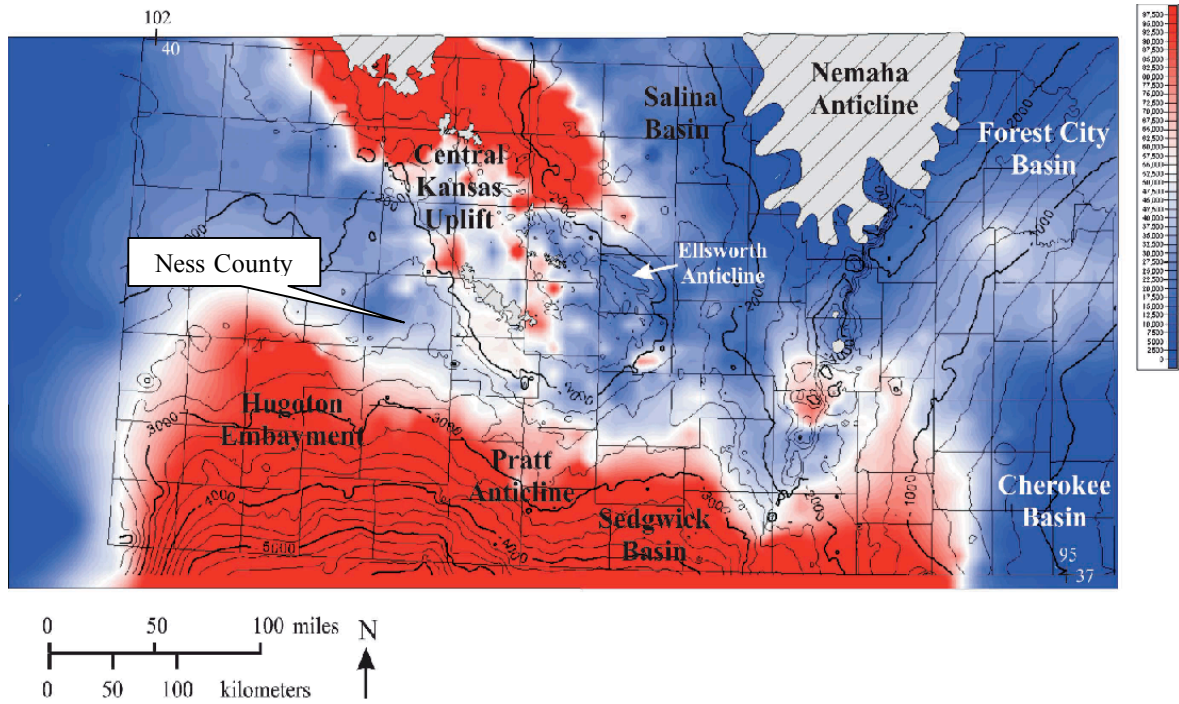


Figure 19: TDS (Total dissolved solids) salinity distribution of deep saline aquifer (Arbuckle Group) in Kansas. Areas where Arbuckle has been removed by erosion are highlighted with gray pattern (Timothy et al (2008)).

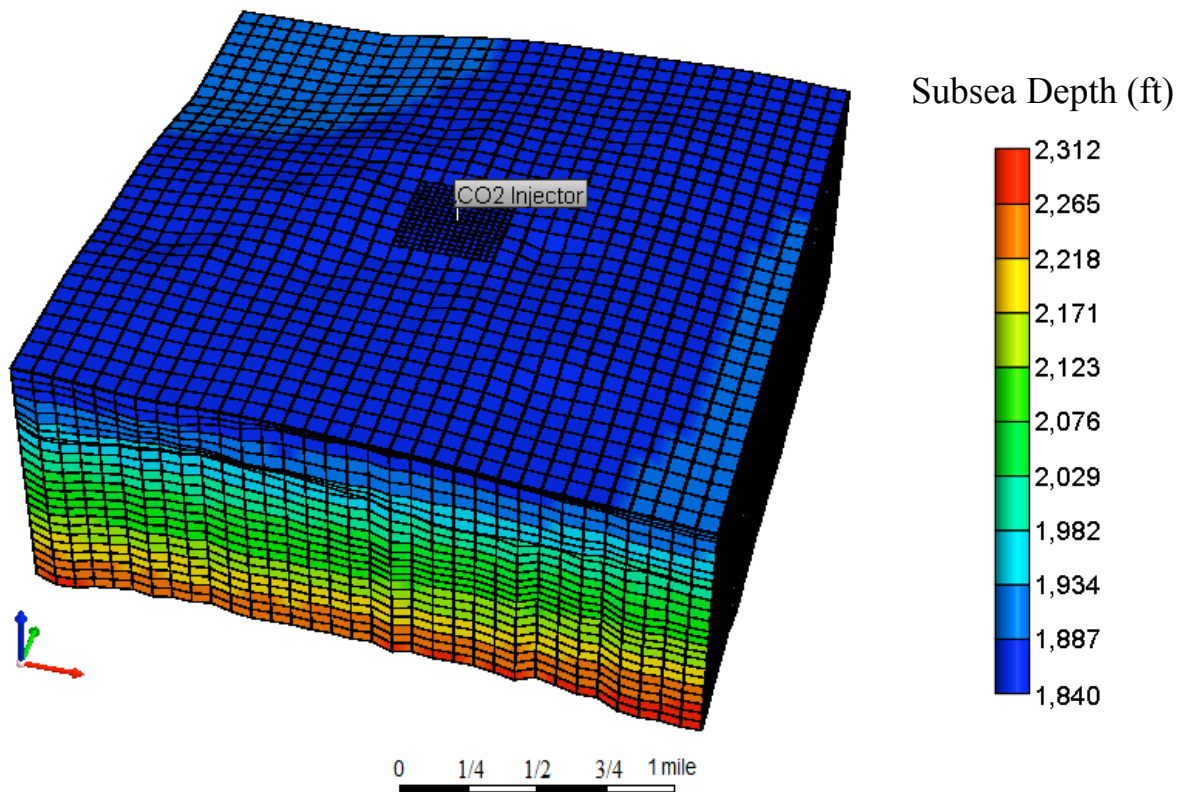


Figure 20: CO₂ sequestration simulation grid with local grid refinement around the injection well. The simulation convergent study was performed on both uniform grid and LGR grid.

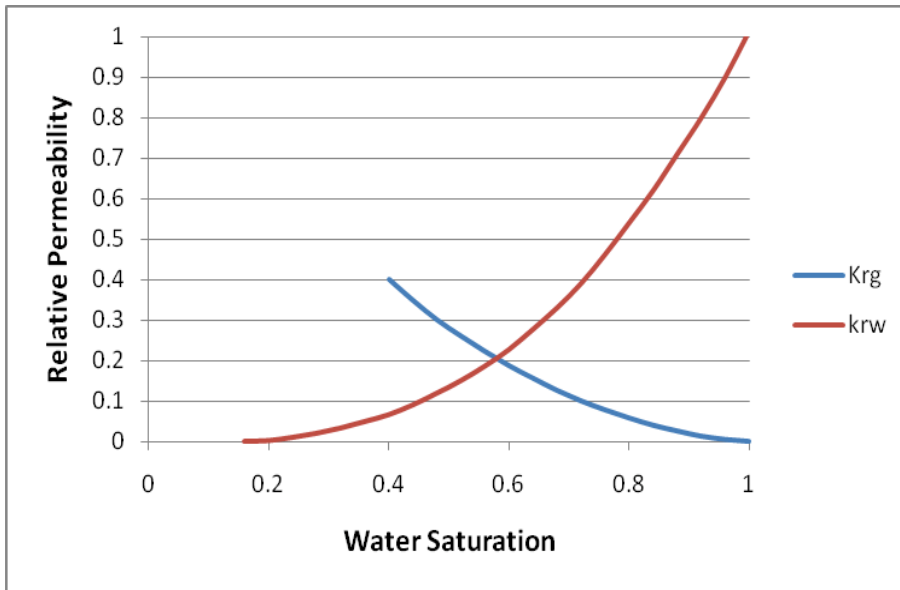


Figure 21: Relative permeability curves for brine and CO₂

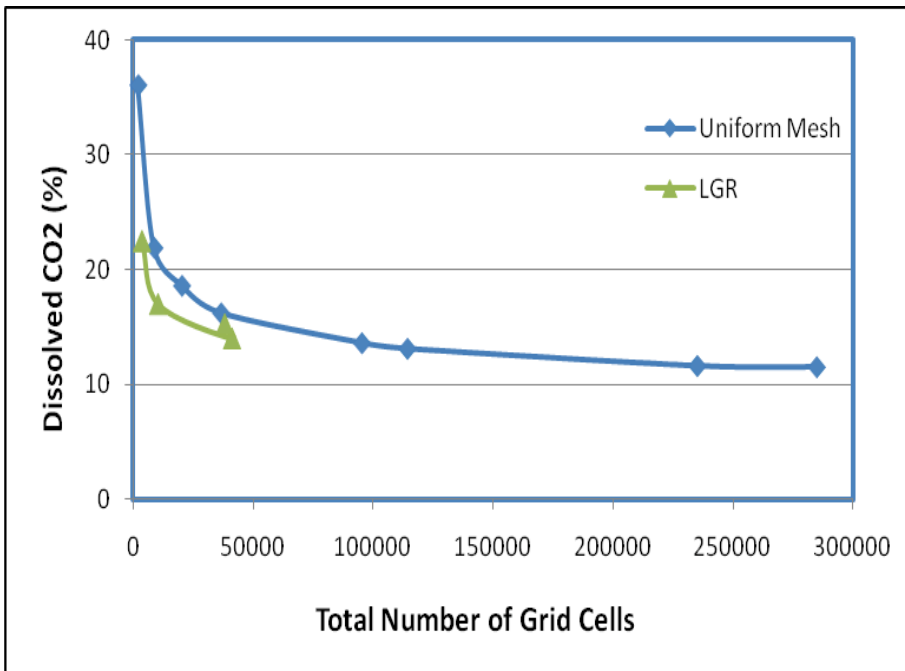


Figure 22: Dickman field simulation grid convergent study for uniform mesh grid and a uniform mesh with local grid refinement (LGR) around the injection borehole.

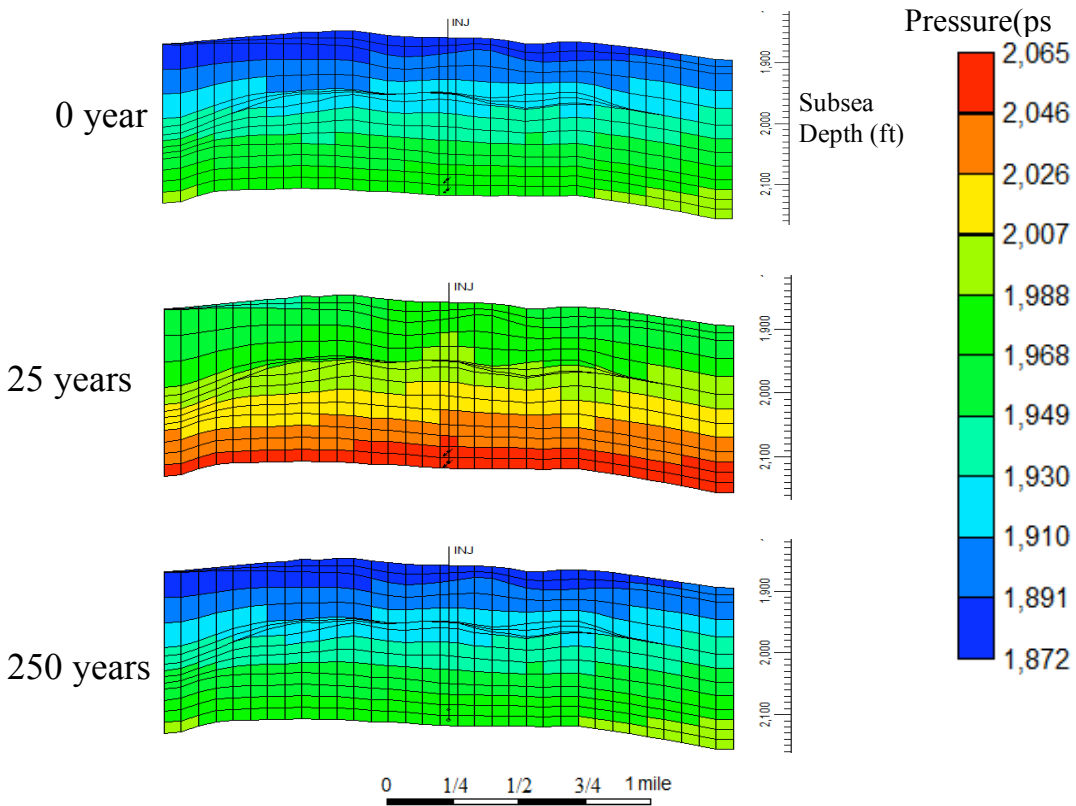


Figure 23. The reservoir pressure distribution before CO₂ injection (top), at the end of the injection (middle), and at the end of simulation. The maximum pressure varies from initial 2007 psi to 2065 psi (middle) and then reduces to the initial pressure.

References

Alan P. B., W. J. Guy, and W. L. Watney, 2002, Characterization of the Mississippian Osage Chat in South-Central Kansas: Kansas Geological Survey, Petroleum Technology Transfer Council workshop presentations,
http://www.pttc.org/workshop_presentations.htm

Carr, T. R., D. F. Merriam, and J. D. Bartley, 2005, Use of relational databases to evaluate regional petroleum accumulation, groundwater flow, and CO₂ sequestration in Kansas, AAPG Bulletin, 89, 12, 1607–1627.

Batzle, M., and Z. Wang, 1992, Seismic properties of pore fluids; Geophysics. 57, 1396-1408.

Li and Liner, 2008, Wavelet-based detection of singularities in acoustic impedances from surface seismic reflection data, Geophysics, 73, V1

Liner, C., 2004, Elements of 3D Seismology, Pennwell Publishing, 608pp.

Kansas Geological Survey, Production maps,
http://crude2.kgs.ukans.edu/DPA/Plays/ProdMaps/miss_sub_gas.html

Merriam D., 1963, Geologic History of Kansas, KGS database, Kansas Geological Survey Bulletin 162, http://www.kgs.ku.edu/Publications/Bulletins/162/08_patt.html

Nghiem, L., C. Yang, V. Shrivatava, B. Kohse, M. Hassam, D. Chen and C. Card, 2009, Optimization of Residual Gas and Solubility Trapping for CO₂ Storage in Saline Aquifer, SPE 119080.

Sifuetes, W, M.J. Blunt, and M. A. Giddins, 2009, Modeling CO₂ Storage in Aquifers: Assessing the Key Contributors to Uncertainty, SPE 123582.

Ziegler P. A., 1989, Evolution of Laurussia — A Study in Late Palaeozoic Plate Tectonics, Kluwer, Dordrecht (1989), p. 102.